Molecular Changes of PET Yarns During Stretching Measured with Rheo-Optical Infrared Spectroscopy and Other Techniques

C. J. M. VAN DEN HEUVEL,* H. M. HEUVEL, W. A. FAASSEN, J. VEURINK, and L. J. LUCAS

Akzo Research Laboratories, Velperweg 76, Postbox 9300, 6800 SB, Arnhem, The Netherlands

SYNOPSIS

A method has been developed for measuring infrared spectra during the mechanical deformation of yarns. This rheooptical technique was applied to study the molecular processes that take place along the stress–strain curve of PET yarns. The results were combined with data obtained from size exclusion chromatography (SEC) and tensile measurements at elevated temperatures. The results indicate that the first modulus maximum marks the breakdown of the amorphous entanglement network and the start of molecular uncoiling by *gauche* → *trans* transitions. In addition, stress develops on the crystals and particularly on tie molecules with a short contour length in the amorphous domains. Ultimately, molecular fracture of taut-tie molecules causes the modulus to pass through a second maximum. The chain ends of broken molecules recoil by *trans* → *gauche* transitions. Local stress accumulation will lead eventually to yarn rupture. © 1993 John Wiley & Sons, Inc.

INTRODUCTION

Technical PET yarns have a complex semicrystalline structure in which polymer molecules are directed along the fiber axis in crystalline and amorphous domains (Fig. 1). Within the crystals, the molecules are well ordered and highly oriented, whereas in the amorphous domains, coiled chains effect an orientation distribution.

Molecules that take part in crystals may run through several crystalline and amorphous regions (tie molecules) or fold back at the surface to reenter the crystal. The chain ends accumulate in the amorphous domains. The above-mentioned molecular ordering gives rise to the formation of so-called fibrils, i.e., structural units in which coherence of amorphous and crystalline domains is found, predominantly in the axial direction.

Although the physical structure of PET yarns can be described in greater detail, the two-phase model has proved to be very useful for characterizing a large number of different yarns in terms of their crystalline morphology, amorphous orientation (distribution), and molecular weight. By combining data obtained from measuring the density, X-ray diffraction patterns, sonic pulse propagation, birefringence, and viscosity, a set of structure parameters can be determined for predicting the mechanical yarn properties quantitatively by means of neural networks.[1,2]

In support of product development, it is worthwhile to supplement this knowledge with a deeper understanding of the molecular processes that characterize the stress–strain curve of the yarn. To that end, infrared spectroscopy seems to be a valuable technique (cf. Refs. 3–19), especially because it provides molecular information about the amorphous domains, which form the weakest links in the physical structure. Furthermore, the rapid scanning capability of Fourier transform infrared (FTIR) has proved useful for measuring the spectral changes that occur during the stretching of polymer films.[9,13,18,19] Therefore, we developed a method for measuring the deformation of yarns with FTIR and

* To whom correspondence should be addressed.

Journal of Applied Polymer Science, Vol. 49, 925–934 (1993)
 CCC 0021-8995/93/050925-10

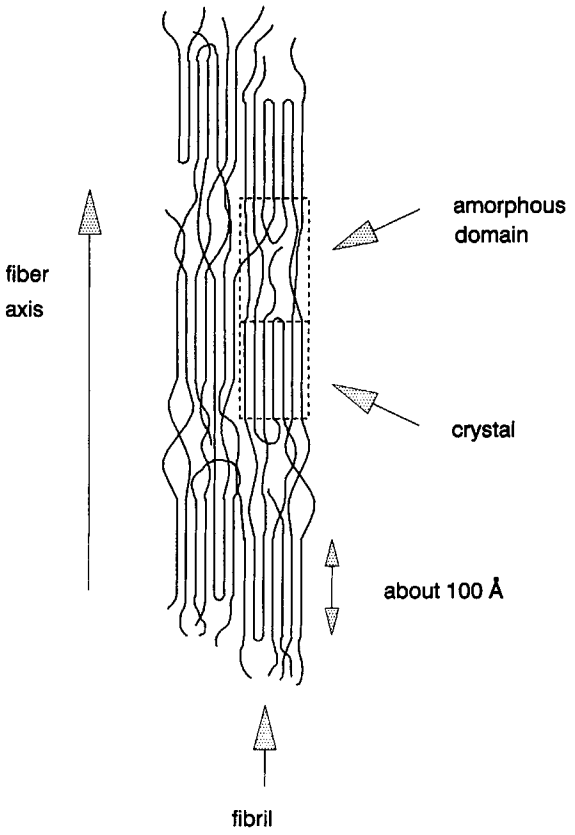

Figure 1 Physical structure of PET yarn.

applied it to PET yarn. The results were combined with data obtained from size exclusion chromatography (SEC) and data on the temperature dependence of the stress–strain curve.

EXPERIMENTAL

The stress–strain experiments were carried out on Akzo Diolen 855T, 1100 dtex f210, a technical PET yarn with a tenacity of 80 cN/tex and an elongation at break of 13% when measured on an Instron tensile tester. Some physical properties of the yarn are, birefringence = 0.1880, sonic modulus = 20.4 GPa, density = 1395.6 kg/m^3 and crystallinity = 0.354.

The sample for the dynamic FTIR experiment was prepared by winding the yarn on a metal frame in such a manner that each side of the frame was covered with a smooth layer of parallel monofilaments with no appreciable air gaps or overlaps (Fig. 2; for details see Ref. 15). The metal frame consisted of two separable parts, so that during stretching in a minitensile tester (Minimat of Polymer Laboratories), all stress was put on the yarn filaments (Fig. 3). An elongation rate of 4%/min was applied. The accuracy with which the stress–strain curve could be recorded with the mini tensile tester was some-

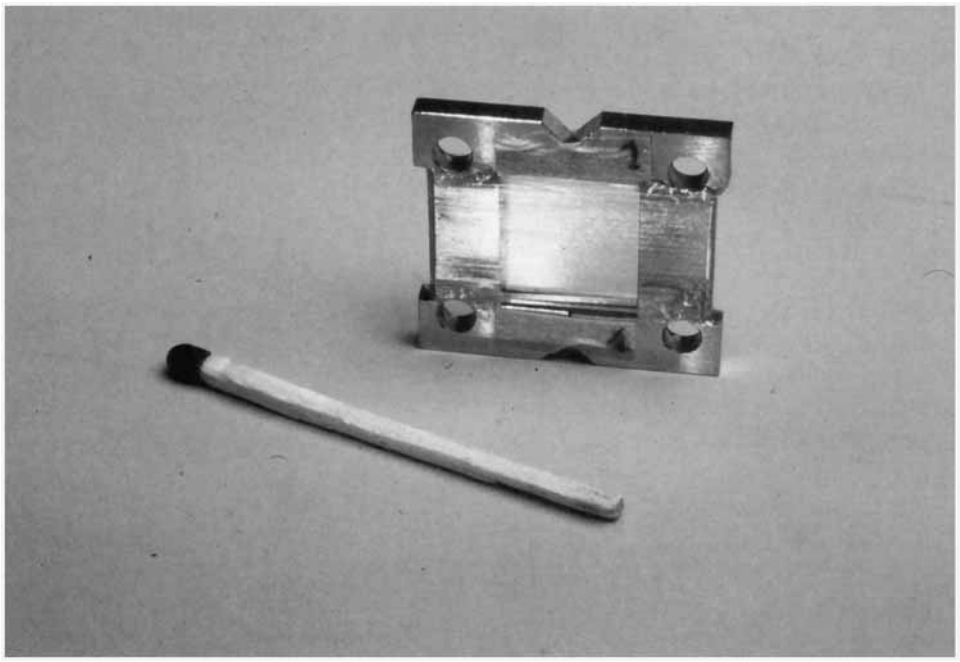

Figure 2 PET filaments wound on a sample holder.

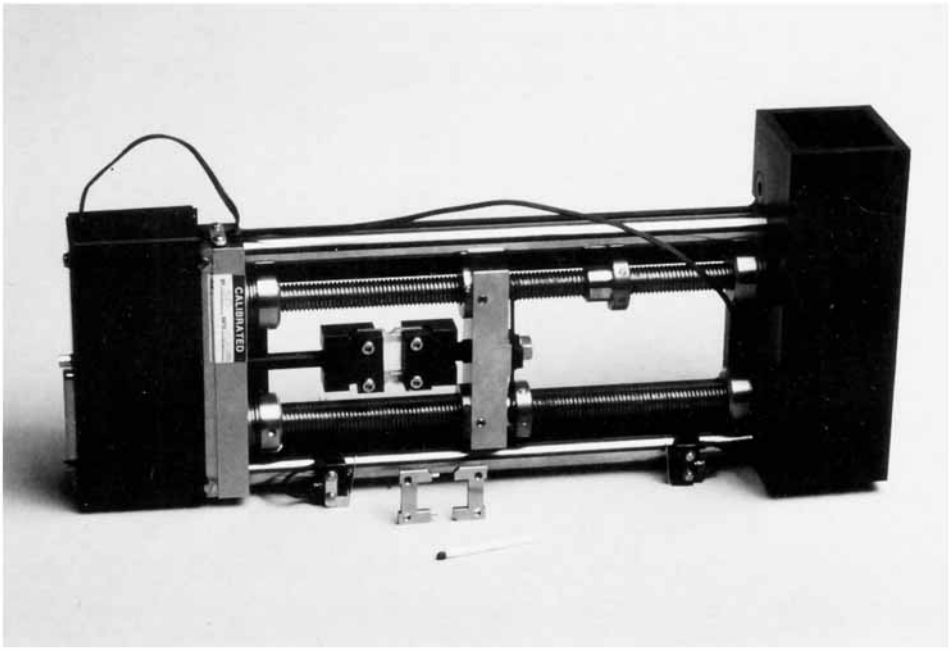

Figure 3 Mini stretching device with clenched PET sample. In front: dismounted sample holder.

what limited and is subject to further study. Nevertheless, the curve has its characteristic shape with the modulus showing two maxima (Fig. 4).

Beforehand, the tensile tester had been placed in a Perkin-Elmer 1800 FTIR instrument with the yarn sample perpendicular to the IR beam (size of the sample was 12 × 25 mm; the image size of the beam had been reduced from 10 to about 8 mm at the sample position). The FTIR spectrometer was equipped with a mercury–cadmium–telluride

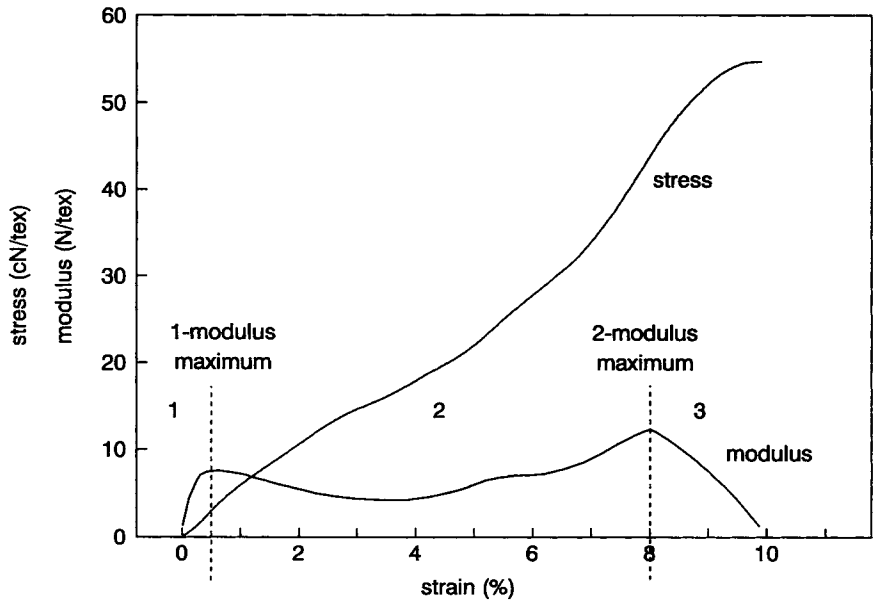

Figure 4 Stress–strain curve of PET yarn.

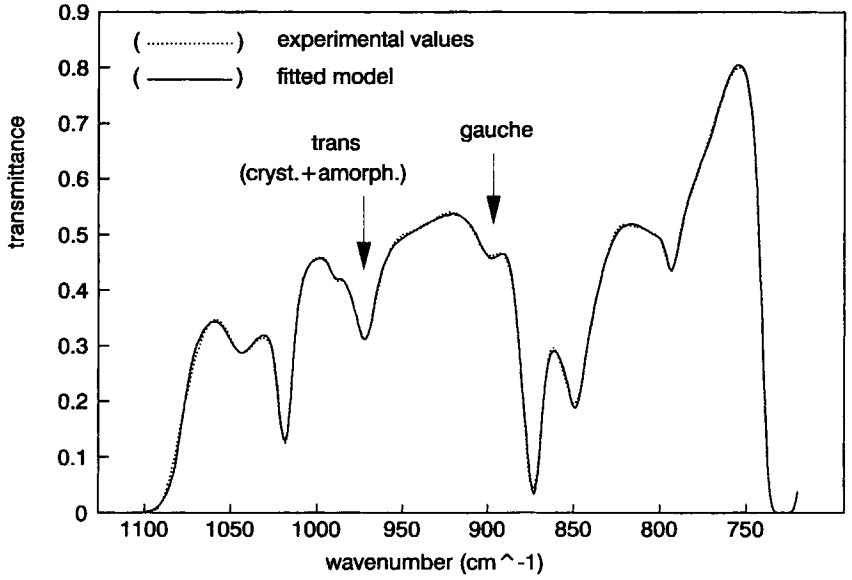

Figure 5 IR spectrum of PET yarn (radiation polarized perpendicular to the yarn axis).

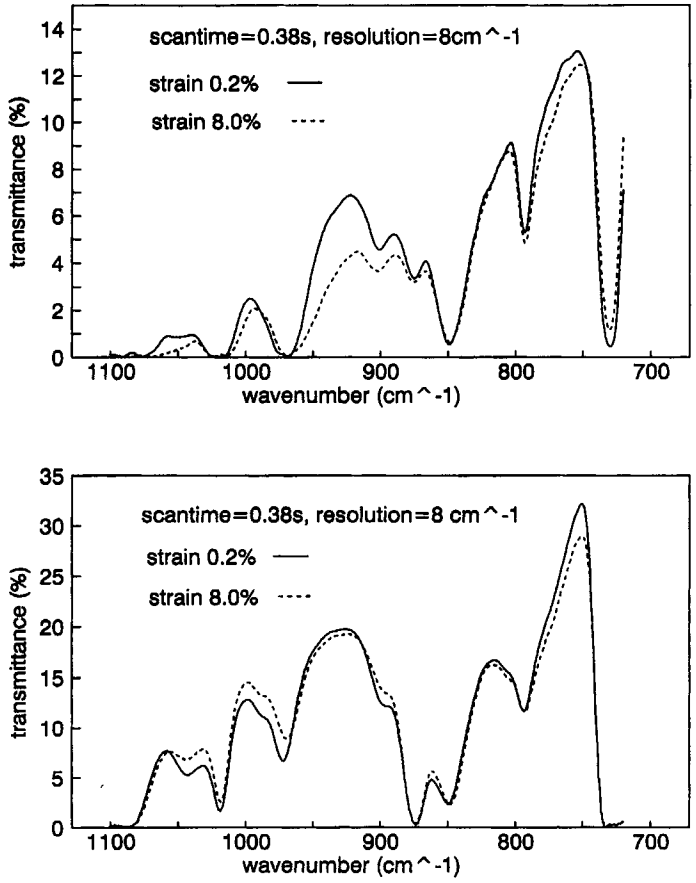

Figure 6 Infrared spectra of PET yarn at a strain of 0.2 and 8.0%, scanned with radiation polarized parallel (above) and perpendicular (below) to the yarn axis.

(MCT) detector and contained a specially designed dynamic polarizer system that made it possible to collect, alternately, spectra with radiation of opposite polarization directions. As a result, each 0.75 s, a pair of high-quality interferograms of the PET yarn could be scanned with the IR radiation polarized parallel and perpendicular to the yarn axis (resolution 8 cm^{-1}). The measurements were stopped when the first filaments broke and leakage of radiation through the sample started to cause spectral distortion. After conversion of the interferograms to the spectra, the spectral region between 700 and 1100 cm^{-1} of each pair of parallel + perpendicular spectra was fitted by means of 23 Pearson functions and the obtained data were combined to quantify the changes of the isotropic area and the positions of the IR bands during stretching (Fig. 5). For a detailed description of this method, we refer to Ref. 15. In Figure 6, two pairs of spectra are shown that were scanned at a strain of 0.2 and 8%.

In a separate experiment, pieces of 50 cm of yarn were stretched in an Instron tensile tester at a rate of 20%/min to various elongation levels ranging from about 1% up to the elongation at break. The molecular weight distribution (MWD) of the samples was determined by size exclusion chromatography (SEC). The SEC analyses were carried out at 32°C using an equipment comprising an HPLC pump, a UV detector operating at a wavelength of 270 nm, and two silica-based columns (pores 1000 and 100 Å, respectively). Hexafluoroisopropanol was used as the eluent. The calibration was done with polytetrahydrofuran standards having molecular weights ranging from 1300 to 300,000.[20]

The measuring of the stress–strain curves at elevated temperatures was carried out with an Instron tensile tester that had been equipped with an oven. The applied gauge length was 25 cm, and the elongation rate, 100%/min.

RESULTS AND DISCUSSION

In Figure 4, the stress–strain curve and its first derivative (the modulus) are shown. Two modulus maxima are present: one at about 0.5% strain and the other at about 8% strain. These two points of maximum resistance to elongation can be used to divide the stress–strain curve into three regions. The molecular changes that take place in the different regions are discussed below.

An important molecular mechanism during straining is the uncoiling of the PET molecules. In this respect, it should be realized that the ethylene groups in the amorphous domains of semicrystalline PET occur in two conformations, namely, the *gauche* and the *trans* conformations. As can be concluded from Figure 7, molecular chains containing a lot of

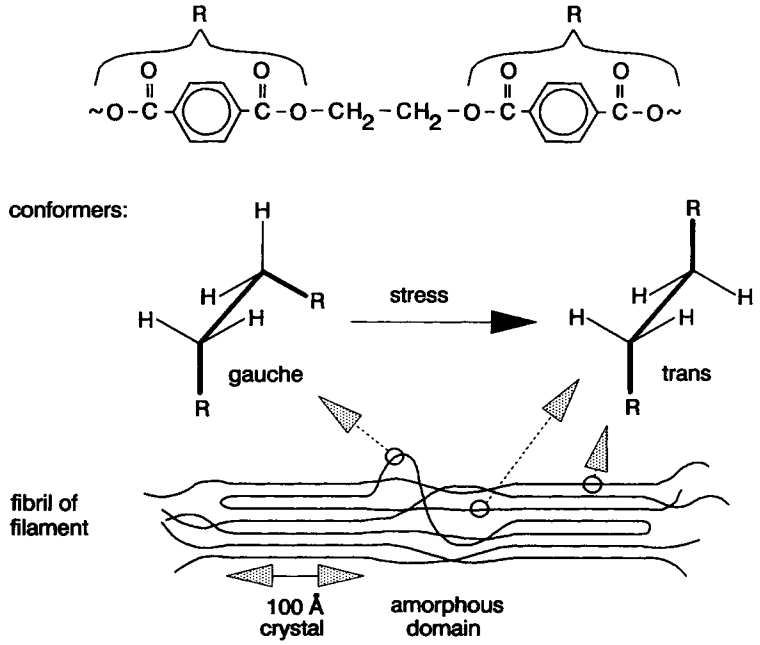

Figure 7 Molecular and physical structure of PET.

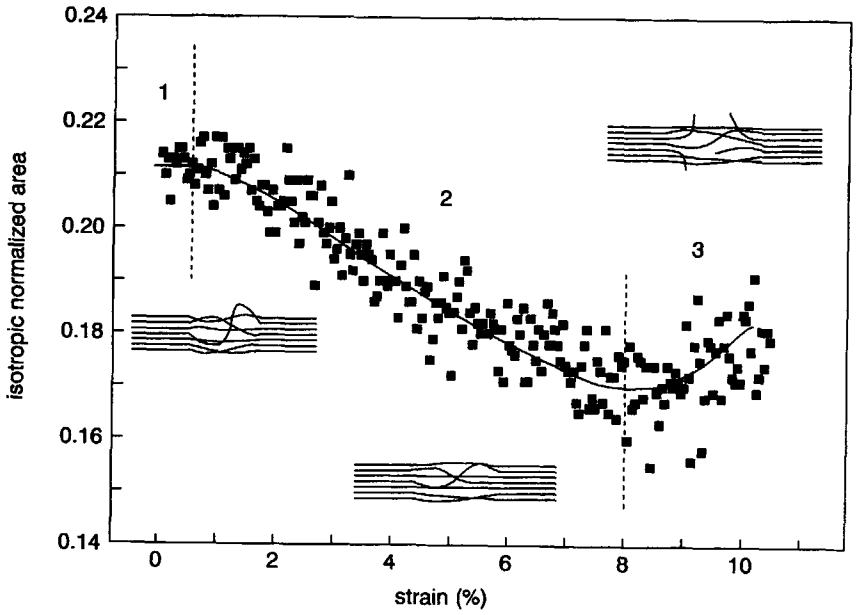

Figure 8 Absorbance of the *gauche* IR band at 899 cm^{-1}.

gauche will be coiled strongly, whereas *trans* conformers in series give rise to extended chains (crystals only contain *trans*). In the infrared spectrum, the amorphous *gauche* conformation can be quantified by means of the CH_2 rocking vibration at about 899 cm^{-1} (Fig. 5). Furthermore, the crystalline and amorphous *trans* conformers show characteristic absorptions at about 970 cm^{-1} as a result of the C—O stretching mode (for band assignments, see Refs. 4, 6, 8, 9, 12, and 15 and references cited therein). The crystalline and amorphous contributions to the *trans* absorption band were separated by the above-mentioned fitting procedure.[15]

When PET yarn is elongated, the molecules tend to align along the fiber axis by uncoiling. Consequently, the amount of *gauche* will diminish.[6,7,8,15,18,19]

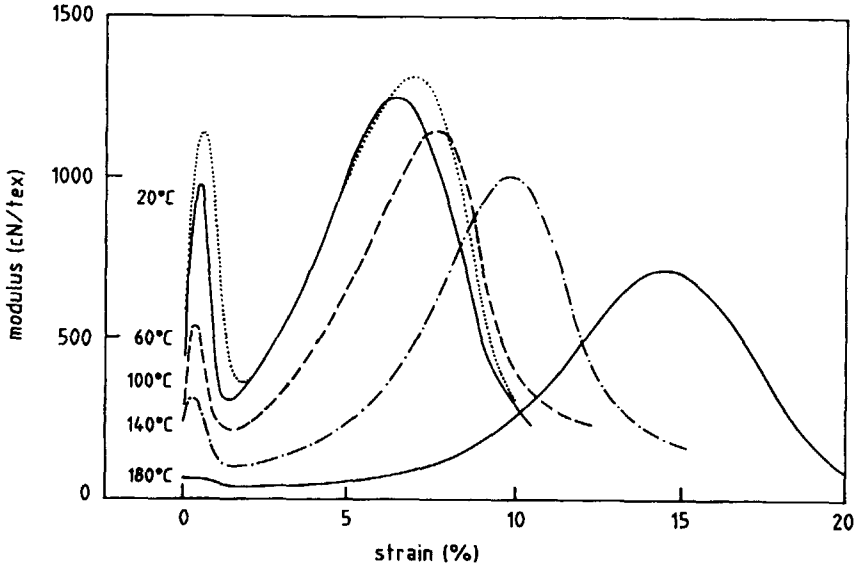

Figure 9 Modulus–strain curves of PET yarn at different temperatures.

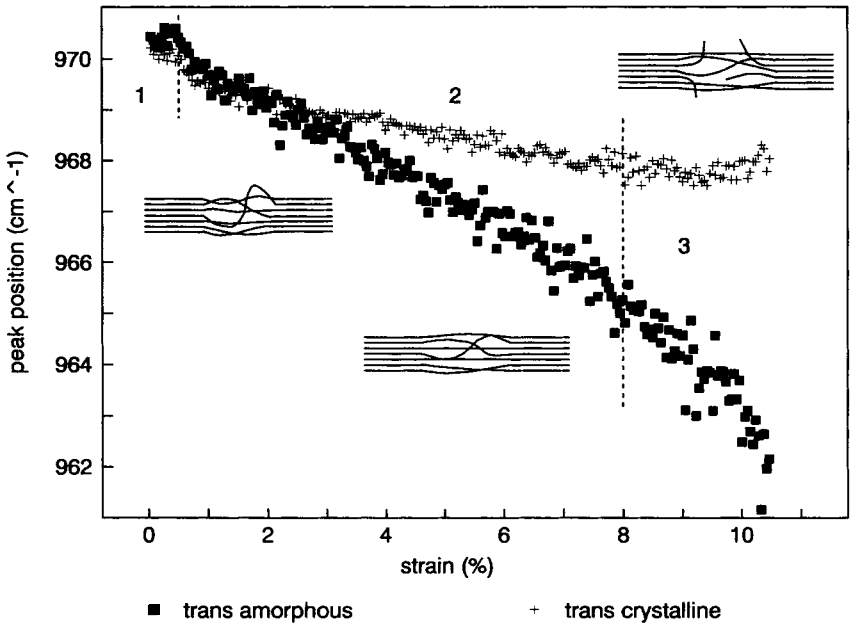

Figure 10 Position of the stress-sensitive *trans* IR band at about 970 cm^{-1}.

A glance at Figure 8 shows that this is indeed the case. On closer examination, it appears that the decrease of *gauche* only starts in region 2 in analogy to earlier findings for PET film.[8] We tentatively believe that in region 1 entanglements (amorphous chain–chain interactions) contribute substantially to the modulus and prevent conformational changes. The elastic strain in this area is probably concentrated in the glycol residues (cf. Ref. 8). The first modulus maximum then marks the breakdown of the entanglement network and the start of molecular uncoiling by *gauche* → *trans* transitions. The weak-

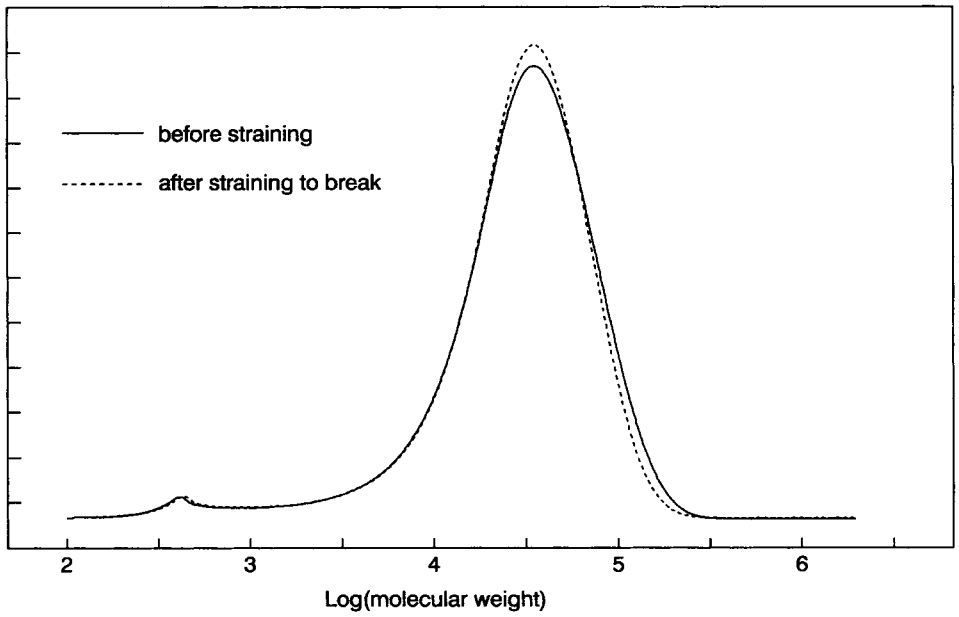

Figure 11 Molecular weight distribution before and after straining to break.

ness of the entanglement network interactions appears from the observation that on increasing the temperature the first modulus maximum of the stress–strain curve collapses around the glass transition temperature of about 80°C (Fig. 9).

The lowering of the tensile modulus in the first part of region 2 can be attributed to the uncoiling of molecular chains in the amorphous domains. In this context, it is worth noting that the tensile modulus is composed of elastic and nonelastic contributions. The elastic contribution as measured by sonic pulse propagation steadily increases in region 2.[21] Therefore, it is reasonable to suppose that uncoiling effects a lowering of the nonelastic modulus.

Preliminary results indicate that the decrease of *gauche* during stretching runs in front of the increase of *trans*, which points to the occurrence of transient skew conformations in between *gauche* and *trans*. Apparently, the glassy state of the amorphous domains hinders the rapid *gauche* ↔ *trans* transitions that occur in solution. This phenomenon is the subject of further study.

Besides the CH2—CH2 *gauche* (G) and *trans* (T) conformers, PET also contains two conformers resulting from the possibility of the two ester groups at the aromatic rings of having a mutual *cis* (C_B) or *trans* (T_B) positioning. In addition, another *gauche* (g) and *trans* (t) conformer arises from rotation about the O—CH2 bond.[12] Fully extended monomer units as present in the crystals and amorphous tautie molecules have the all-*trans* $tTtT_B$ conformational arrangement. It will be clear that during un-

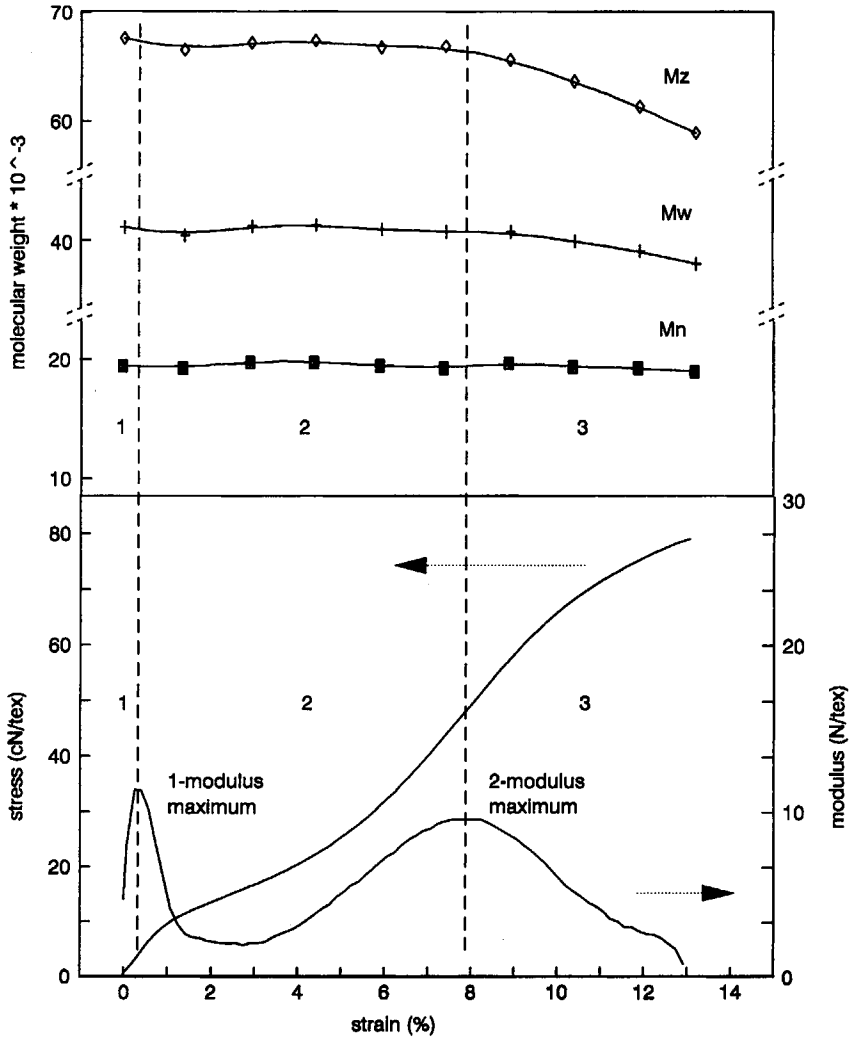

Figure 12 Molecular weight of PET during stretching to break. Different moments of the molecular weight distribution.

coiling the molecules will pass through a large number of different molecular configurations.

The molecular uncoiling in region 2 will ultimately lead to the straining of tie molecules with a short contour length. The strain causes the stretching of covalent bond angles and a downward shift of the *trans* IR band at 970 cm^{-1} (cf. e.g., Refs. 7, 8, 9, and 15). In the present experiment, the position of the band changed considerably, namely, from 971 to 966 cm^{-1} (see also Fig. 6). As mentioned above, the crystalline and amorphous contributions to the *trans* band can be separated by means of fitting. The course of the maxima of the crystalline and amorphous bands is shown in Figure 10. The fact that the shift of crystalline *trans* is smaller than the shift of amorphous *trans* illustrates that the molecules in the crystals bear the load much more collectively than do the amorphous tie molecules, which have a broad contour length distribution.

Since the chain modulus of the taut–tie molecules is relatively high, the tensile modulus of the yarn starts to increase in the second half of region 2. At the point where the modulus reaches its second maximum, taut–tie molecules begin to break, as can be concluded from the lowering of the molecular weight and from the narrowing of the molecular weight distribution (see Figs. 11 and 12; note: the polydispersity M_w/M_n of the molecular weight distribution lowers from 2.1 to 2.0 upon straining to break). Actually, it is the scission of chains that seems to cause the modulus to pass through a maximum. The number of molecules that break, however, is limited (very roughly 3% as calculated from the average molecular weight M_n). Therefore, it is likely that the eventual yarn rupture is initiated in those amorphous regions where, by statistical fluctuations, a high amount of chain scission is realized. Consequently, local stress concentrations are generated, intensifying further accumulation of molecular brcakdown, leading to the ultimate rupture of the filaments.

From Figures 11 and 12 it appears that especially long molecules break (Mz represents especially the molecules with a high molecular weight). This is not surprising because long molecules statistically have the highest chance of breaking. Moreover, they have a short contour length (i.e., a high orientation) due to their long relaxation times during spinning. In Figure 8 it can be seen that beyond the second modulus maximum the amount of *gauche* increases again. Apparently, the breaking of molecules is followed by recoiling of the broken chain ends. Furthermore, the course of the position of the amorphous *trans* IR band in region 3 indicates that the remaining taut–tie molecules are loaded even more heavily (larger IR shift), whereas the crystals somewhat withdraw from the applied strain.

A prerequisite for the aforementioned property of tie molecules to increase the modulus when becoming taut is that they are constrained by crystals. This ability of the crystals to give coherence to the structure will decrease more and more when the temperature approaches the melting point. The modulus then lowers accordingly (Fig. 9).

From the present results it can be concluded that rheooptical FTIR in combination with other measuring techniques can help to provide a clearer insight into the molecular mechanisms governing the mechanical responses during deformation of yarns. In the near future, the equipment and the fitting procedures will be further improved and applied to measuring yarns with a variety of structures and properties.

We want to acknowledge H. Mannee for his important contributions with respect to the fitting of the spectra and Drs. P. van Essen for his work on the mini tensile tester. In addition, we gratefully thank Dr. R. A. Huijts, Dr. M. S. Leloux, and E. L. Meijerink for preparing the strained PET samples and analyzing these samples by size exclusion chromatography. We give special thanks to K. L. A. Flach of Perkin-Elmer Nederland b.v. for his enthusiasm and dedication in designing the dynamic polarizer system.

REFERENCES

1. H. M. Heuvel, L. J. Lucas, C. J. M. van den Heuvel, and A. P. de Weijer, *J. Appl. Pol. Sci.*, **45**, 1649–1660 (1992).
2. R. Huisman and H. M. Heuvel, *J. Appl. Polym. Sci.*, **37**, 595–616 (1989).
3. A. Miyake, *J. Polym. Sci.*, **38**, 479–495 (1959).
4. T. R. Manley and D. A. Williams, *Polymer*, **10**, 339–385 (1969).
5. L. d'Esposito and J. L. Koenig, *J. Polym. Sci. Polym. Phys. Ed.*, **14**, 731–741 (1976).
6. B. Jasse and J. L. Koenig, *J. Macromol. Sci.-Rev. Macromol. Chem.*, **C17**(1), 61–135 (1979).
7. S. S. Sikka and H. H. Kausch, *Colloid Polym. Sci.*, **257**, 1060–1067 (1979).
8. I. J. Hutchinson, I. M. Ward, H. A. Willis, and V. Zichy, *Polymer*, **21**, 55 (1980).
9. H. W. Siesler and K. Holland-Moritz, *Infrared and Raman Spectroscopy of Polymers; Practical Spectroscopy Series*, Marcel Dekker, New York, 1980, Vol. 4; ISBN 0-8247-6935-X.

10. A. Garton, D. J. Carlsson, and D. M. Wiles, *Text. Res. J.*, 28 (1981).
11. S.-B. Lin and J. L. Koenig, *J. Polym. Sci. Polym. Phys. Ed.*, **20,** 2277–2295 (1982).
12. J. Stokr, B. Schneider, D. Doskocilova, J. Lövy, and P. Sedlacek, *Polymer,* **23,** 714 (1982).
13. H. W. Siesler, *Adv. Polym. Sci.*, **65,** 2–72 (1984).
14. F. Rietsche and B. Jasse, *Polym. Bull.*, **11,** 287–292 (1984).
15. H. M. Heuvel and R. Huisman, *J. Appl. Polym. Sci.*, **30,** 3069–3093 (1985).
16. I. M. Ward, *Adv. Polym. Sci.*, **66,** 82–115 (1985).
17. M. Yazdanian, I. M. Ward, and H. Brody, *Polymer,* **26,** 1779 (1985).
18. V. B. Gupta and C. Ramesh, *J. Polym. Sci. Polym. Phys. Ed.*, **23,** 405–411 (1985).
19. H. W. Siesler, *Makromol. Chem. Maccromol. Symp.*, **53,** 89–103 (1992).
20. A detailed description of the applied method will be published by F. A. Buijtenhuijs of Akzo Research Laboratories.
21. J. G. M. van Miltenburg, *Text. Res. J.*, **61,** 363–369 (1991).

Received September 15, 1992
Accepted November 24, 1992